

Research Paper

HSP90 Inhibitor Encapsulated Photo-Theranostic Nanoparticles for Synergistic Combination Cancer Therapy

Tzu-yin Lin^{1*}, Wenchang Guo^{2*}, Qilai Long³, Aihong Ma⁴, Qiangqiang Liu⁴, Hongyong Zhang¹, Yee Huang⁴, Siddarth Chandrasekaran⁴, Chongxian Pan^{1,5}, Kit S. Lam^{1,4}, Yuanpei Li⁴

1. Department of Internal Medicine, Division of Hematology/Oncology, University of California Davis, Sacramento, CA 95817, USA;
2. Department of Pathology, Keck School of Medicine, University of Southern California, Los Angeles, CA 90033, USA;
3. Department of Urology, Zhongshan Hospital, Fudan University, Shanghai, 200032, China;
4. Department of Biochemistry and Molecular Medicine, UC Davis Comprehensive Cancer Center, University of California Davis, Sacramento, CA 95817, USA;
5. VA Northern California Health Care System, Mather, CA, USA.

*Authors contributed equally to this work.

✉ Corresponding authors: Kit S. Lam (kslam@ucdavis.edu) and Yuanpei Li (lypli@ucdavis.edu).

© Ivyspring International Publisher. Reproduction is permitted for personal, noncommercial use, provided that the article is in whole, unmodified, and properly cited. See <http://ivyspring.com/terms> for terms and conditions.

Received: 2016.01.04; Accepted: 2016.05.01; Published: 2016.06.07

Abstract

Photodynamic therapy (PDT) is a promising non-invasive therapeutic modality that has been proposed for treating prostate cancer, but the procedure is associated with limited efficacy, tumor recurrence and photo-toxicity. In the present study, we proposed to develop a novel multifunctional nano-platform for targeted delivery of heat, reactive oxygen species (ROS) and heat shock protein 90 (Hsp90) inhibitor simultaneously for combination therapy against prostate cancer. This new nano-platform combines two newly developed entities: 1) a unique organic and biocompatible nanoporphyrin-based drug delivery system that can generate efficient heat and ROS simultaneously with light activation at the tumor sites for dual-modal photothermal- and photodynamic- therapy (PTT/PDT), and 2) new nano-formulations of Hsp90 inhibitors that can decrease the levels of pro-survival and angiogenic signaling molecules induced by phototherapy, therefore, further sensitizing cancer cells to phototherapy. Furthermore, the nanoparticles have activatable near infrared (NIR) fluorescence for optical imaging to conveniently monitor the real-time drug delivery in both subcutaneous and orthotopic mouse models bearing prostate cancer xenograft. This novel multifunctional nano-platform has great potential to improve the care of prostate cancer patients through targeted combination therapy.

Key words: Nano-theranostics, Hsp90 inhibitor, Photo-therapy, Combination therapy, Prostate cancer.

Introduction

Prostate cancer is the second leading cause of all cancer-related deaths and the most commonly diagnosed cancer among males in the US (2/3 of the patients are older than 65). In practice, many elderly patients are not offered curative treatment options such as radical prostatectomy or radiotherapy. Patients with prostate cancer who elect to undergo definitive radiotherapy have limited options for salvage therapy after local treatment failure. Moreover, first-line, definitive management of early stage prostate cancer with either surgery or radiotherapy has significant associated morbidities

due to the proximity of normal structures such as nerves, bladder, and rectum[1, 2]. The search for effective and safe therapeutic agents for prostate cancer is a relevant and timely pursuit. The intrinsically defined area of photodynamic therapy (PDT) imposed by near-infrared (NIR) light has the potential to selectively treat the prostate while sparing the surrounding normal tissues [1, 2]. By adapting the techniques developed for interstitial brachytherapy with radioactive seeds, light can be delivered to the entire prostate gland using interstitial, cylindrically diffusing optical fibers. Unlike chemotherapy or

radiotherapy, the mechanism of cell killing by PDT is not dependent on DNA damage or cell cycle effects, decreasing the chances of therapy cross-resistance and eliminating late normal tissue effects such as treatment-induced second malignancy. Together, these factors make prostate cancer an attractive target for clinical photo-therapy development. Although promising, one main limitation associated with current PDT approach is that the photosensitizers have poor pharmacokinetic (PK) characteristics and selectivity between tumor and normal tissues resulting in limited efficacy and significant photo-toxicity[3-7]. Furthermore, PDT alone was found to induce expression of various pro-survival and angiogenic signaling molecules (e.g. HIF-1 α , survivin, Akt, MMP-2 and VEGF) in tumor tissue, which can reduce its efficacy [1, 2, 8, 9].

The Hsp90 inhibitors, such as 17-allylamino-17-demethoxygeldanamycin (17AAG) and 17-(dimethylaminoethylamino)-17-demethoxygeldanamycin (17DMAG), could inhibit most of the pro-survival and angiogenic signaling molecules elevated by PDT. Therefore, combination of Hsp90 inhibitors with PDT has a great potential to improve the efficacy of PDT [1, 2, 8, 9]. Hsp90 is an attractive anticancer drug target [10, 11]. Hsp90 in tumor cells is present in multi-chaperone complexes with high ATPase activity and this form was found to bind to 17AAG with 100 times greater affinity than the latent, inactive form of Hsp90 in normal cells [10]. Inhibition of Hsp90 causes depletion of a number of oncoproteins and could attack all six "hallmarks" of cancer simultaneously[12]. These properties give Hsp90 inhibitors advantages over other signal-blocking antitumor agents. Many single signal targeting agents lack clinical activity due to quick drug resistance of cancer cells, while no drug resistance has been observed for Hsp90 inhibitors. More interestingly, inhibition of Hsp90 leads to the depletion of androgen receptor (AR), a client protein of Hsp90, in prostate cancer cells[13]. 17AAG has been proven to be efficacious in animal models and in early phase clinical trials of prostate cancer. However, issues on formulation difficulty and vehicle related toxicity have prevented 17AAG from moving to phase 3 clinical trials.

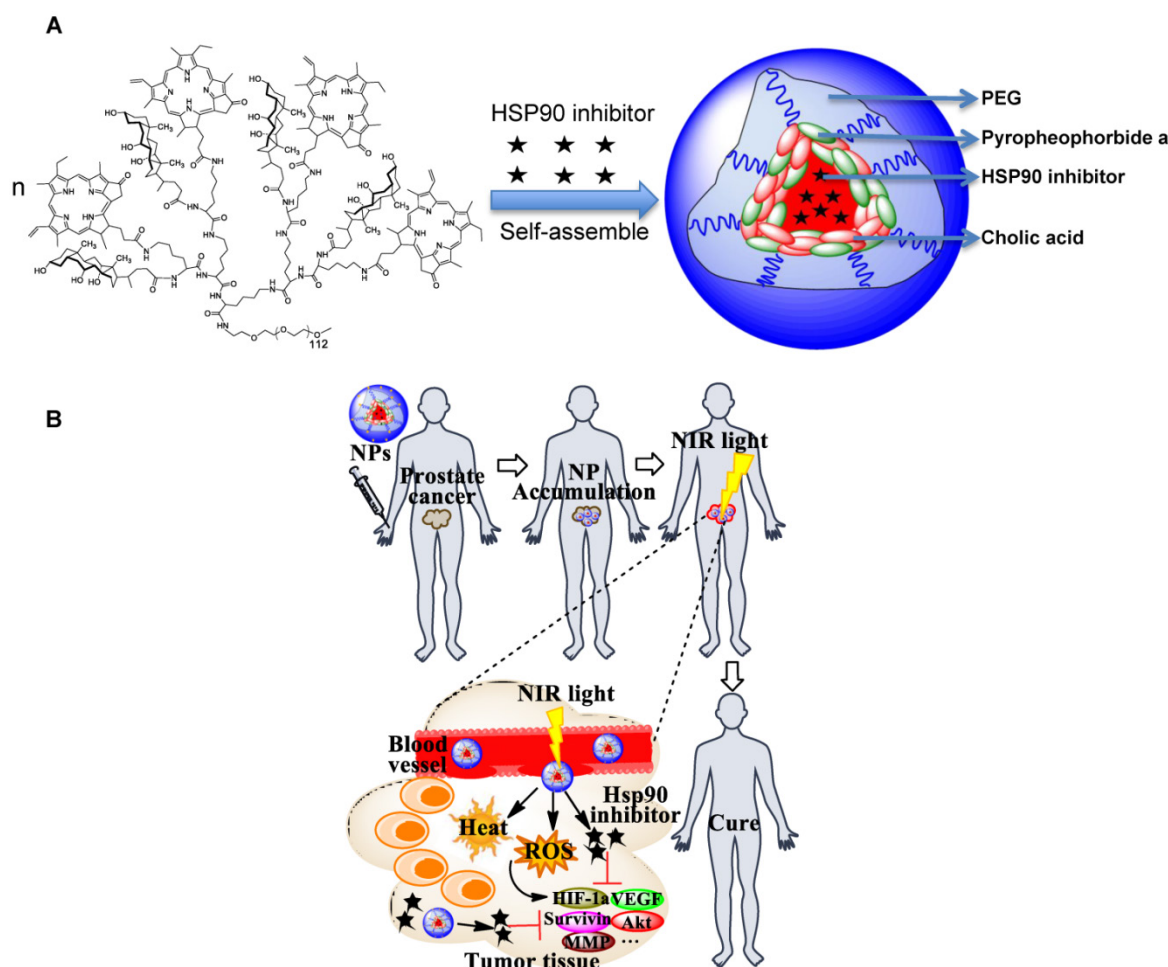
"All-in-one" nanoparticles based on aggregated porphyrins have attracted considerable attentions for their potential applications in cancer imaging and therapy. For instance, liposomal nanovesicles based on the supramolecular assembly of porphyrin-lipids (named Porphysomes) pioneered by Zheng group have shown exciting photonic properties as well as multimodal imaging capability [14, 15]. Our group recently reported the development of an unique

micelle-based nanoporphyrin platform, for the integration a broad range of imaging and therapeutic functions that include near infra-red fluorescence imaging (NIRFI), positron emission tomography (PET), magnetic resonance imaging (MRI), PDT, photothermal therapy (PTT), and targeted drug delivery[16]. Nanoporphyrins have unique architecture-dependent photothermal- and photodynamic- properties. Upon illumination with a portable low energy NIR light, nanoporphyrins could be activated to release ROS, heat and drugs simultaneously at tumor sites in transgenic and xenograft murine models, leading to complete eradication of tumors. Recently, we have demonstrated that our novel nanocarriers could be used to encapsulate Hsp90 inhibitors such as 17AAG with very high efficiency. We hypothesize that nanoporphyrin-mediated PTT/PDT will have synergistic effects with targeted molecular therapy using Hsp90 inhibitors for the treatment of prostate cancer (**Scheme 1A &B**).

Materials and Methods

Preparation and characterization of Hsp90 inhibitor loaded nanoporphyrins

Porphyrin-based telodendrimer was synthesized via solution phase condensation reaction according to our published methods[16]. Hsp90 inhibitors, e.g. 17AAG or 17DMAG, were loaded into nanoporphyrins via "dry-down method"[17-20], in which the drugs and telodendrimers were dissolved in methanol, dried down, re-suspended and sonicated in PBS, and followed by ultra-centrifugation. The drug loading was calculated according to the calibration curve between the HPLC area values and concentrations of drug standard. The loading efficiency is defined as the ratio of drug loaded into micelles to the initial drug content. The size and size distribution of drug loaded nanoporphyrins were measured by dynamic light scattering (DLS, Microtrac). The concentration of nanoporphyrins was kept at 1.0 mg/mL for DLS measurements. All measurements were performed at 25 °C, and data were analyzed by Microtrac FLEX Software 10.5.3. The near infrared fluorescence of nanoparticle solutions (10 μ L) was scanned using a Kodak multimodal imaging system IS2000MM. The photothermal property of nanoparticle solutions (10 μ L) was studied using a FLIR thermal camera. The production of reactive oxygen species (ROS) from nanoparticle solutions was monitored using singlet oxygen sensor green (SOSG, Invitrogen) as an indicator as described previously[21, 22].



Scheme 1. Schematic illustration of Hsp90 inhibitor loaded nanoporphyrins (**A**) and their application for combination prostate cancer therapy (**B**).

Cellular uptake of NP-AAG by flow cytometry and confocal microscopy

PC3 cells were treated with 17AAG loaded nanoporphyrin (NP-AAG) (nanoporphyrin: 10 $\mu\text{g}/\text{mL}$, 17AAG: 8 $\mu\text{g}/\text{mL}$) for 20 minutes. Cells were fixed in the 10% formalin on ice for 1 hour and analyzed by flow cytometry. For confocal imaging, PC3 cells were cultured on the 8 well chamber slides overnight. Samples were treated with NP-AAG (1:50) containing DAPI (nucleus staining, Invitrogen) for 2 hours. Imaging was acquired by Zeiss confocal microscopy without wash or fix.

In vitro ROS production

We first treated PC3 cells with 1.0 mg/mL of NP-AAG for 24 h followed by 30 min loading with 2',7'-dichlorofluorescein diacetate (DCF-DA, Invitrogen) as an indicator in complete medium (to facilitate cellular uptake) in 8-well chamber slides to monitor the ROS production[16]. Cells were washed three times with PBS and replaced with fresh medium with DAPI. Imaging was acquired before and after illumination with NIR light (0.07 W cm^{-2} for 60 s)

under the same field as fluorescence microscopy, using the Metamorph program to investigate the ROS production.

Cell survival and apoptosis assays

PC3 and LNCAP prostate cancer cell lines and RPWE1 normal prostate cell line were used to evaluate the photosensitizing function of NP-AAG in comparison with nanoporphyrin alone and free drug 17AAG. Cells were seeded at 5000 cells/50 μl /well overnight and then treated with the corresponding drugs at the indicated concentrations for 24 hrs. The drugs were then removed and replaced with fresh medium, and the cells were exposed to NIR light for 2 minutes. Growth inhibition was measured after another 72 hours using a 3-(4,5-dimethylthiazol-2-yl)-2,5-diphenyltetrazolium bromide (MTT) assay (Roche Diagnostic, Mannheim, Germany) according to the manufacture's protocol. The fraction of affect (Fa) Combination index (CI) plot of each cell line treated with NP-AAG mediated photodynamic therapy was determined. $\text{CI} < 1$ is considered synergistic, while $\text{CI} < 0.3$ is considered strong

synergistic. CI was calculated with Compusyn software based on Chou-Talalay method [23, 24]. Regarding apoptosis assay, PC3 cells were seeded at 5×10^5 /well overnight and then treated with PBS, nanoporphyrin, or NP-AAG for 24 hours followed by washing with PBS. Cells were treated with NIR light for 2 minutes. 24 hours later, cells undergoing apoptosis were identified using annexin V-FITC kit (Abcam), following the manufacturer's instructions. The cells were analyzed using a Coulter Epics XL flow cytometer (Beckman Coulter, Miami, FL).

Western Blot

Western blotting was performed as described previously [25]. PC3 cells were grown in 100 mm dishes to about 50% confluence, treated with PBS, nanoporphyrin and NP-AAG for 6 hours and then replaced with fresh medium followed by 2 minutes of NIR light. 12 hours later, cells were collected and lysed in the lysis buffer. Proteins were detected by the following antibodies: HIF1 α , Survivin, AKT, MMP2, Src (2109) (Cell signaling Technology) and β -actin (Sigma-Aldrich, A1978).

Xenograft and Orthotopic mouse prostate cancer model

All animals were kept under pathogen-free conditions according to AAALAC guidelines and were allowed to acclimatize for at least 4 days prior to any experiments. All animal experiments were performed in compliance with institutional guidelines and according to protocol No. 07-13119 and No. 09-15584 approved by the Animal Use and Care Administrative Advisory Committee at the University of California Davis. For both subcutaneous and orthotopic xenograft models, male athymic nude mice (Nu/Nu strain), 6-8 weeks age, were purchased from Harlan (Livermore, CA). The subcutaneous xenograft model of prostate cancer was established by injecting 2×10^6 PC3 cells in a 100 μ L of mixture of PBS and Matrigel (1:1 v/v) subcutaneously into the right flank of male nude mice. PC3 cells were implanted into the ventral prostate lobe of mice for orthotopic models as described previously [26].

In vivo mouse optical imaging

Mouse models bearing subcutaneous and orthotopic PC3 prostate cancer xenograft were used for *in vivo* imaging study. Mice were intravenously injected with NP-AAG. 72 hours later, animals were sacrificed and NIR fluorescence imaging were acquired using a Kodak multimodal imaging system IS2000MM (Kodak). For orthotopic model, an incision was made to expose organs and orthotopic tumors after euthanasia for whole mouse NIR imaging. After imaging, mice were sacrificed and tumor and other

organs were excised for *ex vivo* imaging.

In vivo therapeutic efficacy and toxicity study of NP-AAG in prostate cancer xenograft model

PC3m xenograft bearing mice were established as previously described. After tumor reached 50-100 mm³ in size, they were randomly assigned to receive PBS, 17AAG (40mg/kg), nanoporphyrin (2 groups, 50 mg/kg nanoporphyrin), and NP-17AAG (40mg/kg 17AAG, 50mg/kg nanoporphyrin). 24 hours post-injection, tumors in nanoporphyrin groups were treated with high dose of light (1.25 W/cm², 680nm) for 3 minutes, while tumor in second nanoporphyrin group and NP-AAG were treated with 0.5 W/cm² light for 3 minutes. Tumor surface temperatures were monitored with a thermal camera (FLIR). The temperature readings in the central point of the illumination area were recorded continuously. Mice were given treatment once per week for a total of 3 weeks. Tumor sizes were measured with a digital caliper twice per week. Tumor volume was calculated by the formula $(L \cdot W^2)/2$, where L is the longest and W is the shortest in tumor diameters (mm). Relative tumor volume (RTV) equals the tumor volume at given time point divided by the tumor volume before initial treatment. Mice behaviors and skin ulceration was monitored daily, while body weight was documented twice a week. On the third day after the last dose, blood samples were obtained from all mice for measurement of complete blood count (CBC), alanine aminotransferase (ALT), aspartate aminotransferase (AST), total bilirubin, blood urea nitrogen (BUN), total bilirubin, and creatinine.

Statistical analysis

Statistical analysis was performed by Student t test for two groups, and one-way ANOVA for multiple groups. All results were expressed as the mean \pm standard error of mean (SEM) unless otherwise noted. P value less than 0.05 was considered statistically significant.

Results

Synthesis and characterization of NP-AAG

17AAG could be efficiently encapsulated into our previously reported nanoporphyrim[16] for combination therapy. The drug loading efficiency was approaching 100% with a 17AAG concentration at 4.0 mg/mL. Dynamic light scattering (DLS) showed the particle size of 17AAG-loaded nanoporphyrim (NP-AAG) to be about 22 ± 8 nm (Fig. 1A,B), which is very similar to the empty nanoporphyrim[16]. The morphology of NP-AAG was spherical as observed under transmission electron microscopy (TEM) (Fig. 1C). Furthermore, NP-AAG retained the

architecture-dependent fluorescence property, photodynamic- and photothermal- transduction property of empty nanoporphyrin. The NIR fluorescence of NP-AAG was very low when NP-AAG retains their micellar integrity in PBS (**Fig. 1D**), indicating the strong self-quenching effect of the excited state in the aqueous medium. The NIR fluorescent signal of the NP-AAG was greatly amplified when the drug loaded nanoparticles were disrupted by sodium dodecyl sulfate (SDS)[19, 27] (**Fig. 1D**). Similarly, the photodynamic transduction

of NP-AAG in PBS was very low, but could be restored with SDS, measured by the ROS generation using SOSG as an indicator (**Fig. 1E**) [21, 22]. To the contrary, illuminated with the same dose of light, the temperature changes (ΔT) of NP-AAG solution in PBS was significantly higher than that in the presence of SDS, as NP concentrations increased from 0 to 1.0 mg/mL (**Fig. 1F**). These observations indicated that NP-AAG possessed similar architecture-dependent photothermal-transduction property as our previously reported nanoporphyrins[16].

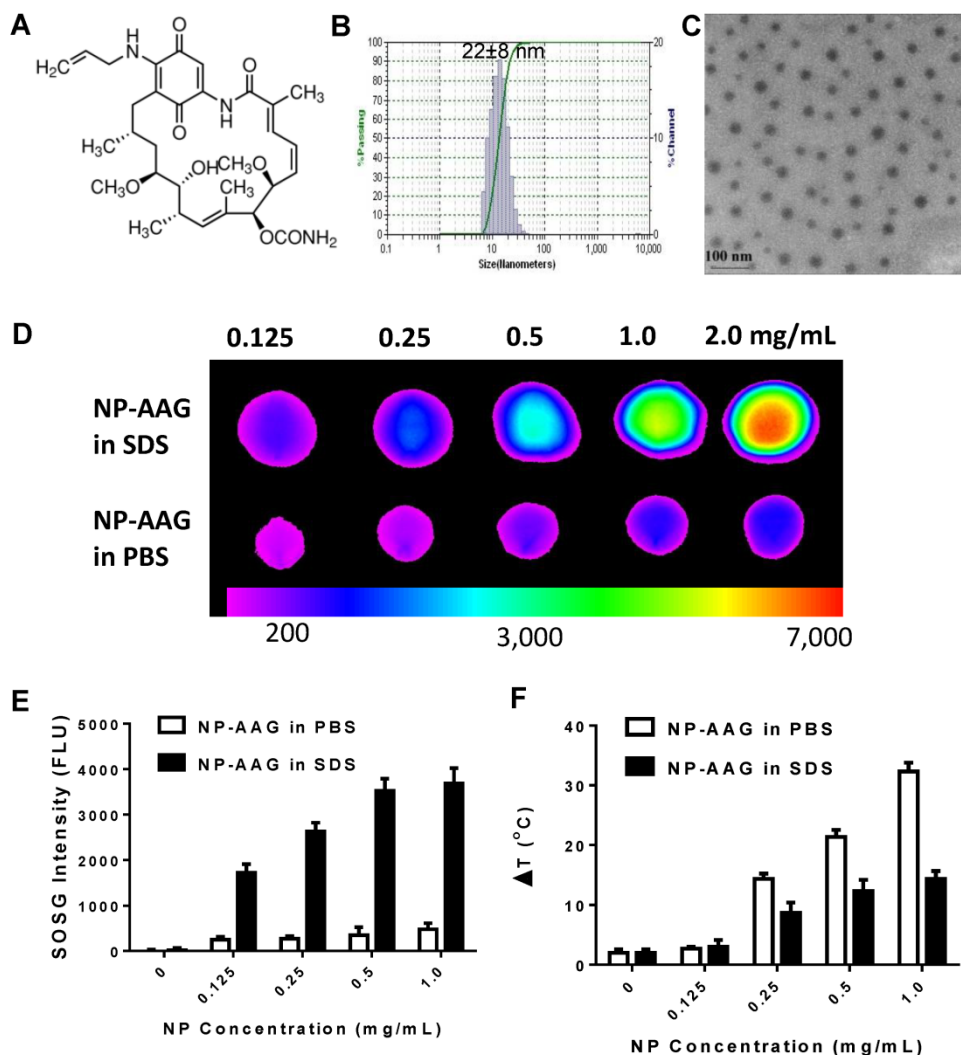


Figure 1. (A) The chemical structure of 17-allylamino-17-demethoxygeldanamycin (17AAG)[1, 2, 8, 9]. (B) The particle size of 17AAG loaded nanoporphyrins (NP-AAG). The loading level of 17AAG in NP-AAG was 4 mg/mL as determined by HPLC. The particle size was measured by dynamic light scattering (DLS) and the data was analyzed by Microtrac FLEX Software 10.5.3. The particle size data was shown as average particle size \pm Standard Deviation (SD) based on three measurements. (C) TEM image of NP-AAG (stained with phosphotungstic acid, PTA). Scale bar: 100 nm. (D) Near-infrared fluorescence imaging of NP-AAG solution (10 μ L) in the absence and in the presence of SDS acquired using a Kodak multimodal imaging system IS2000MM (Kodak) with an excitation bandpass filter at 625/20 nm and an emission filter at 700/35 nm. (E) Single oxygen generation of NP-AAG in PBS and SDS upon light irradiation (690 nm at 0.25 w/cm² for 60 seconds) measured by using SOSG as an indicator[21, 22] (n=3). (F) Concentration-dependent photo-thermal transduction of NP-AAG: quantitative temperature change (ΔT) (n=2). The temperature of NP-AAG solution (10 μ L) in the absence and in the presence of SDS was monitored by a thermal camera after irradiation with NIR laser (690 nm) at 1.25 w/cm² for 20 seconds.

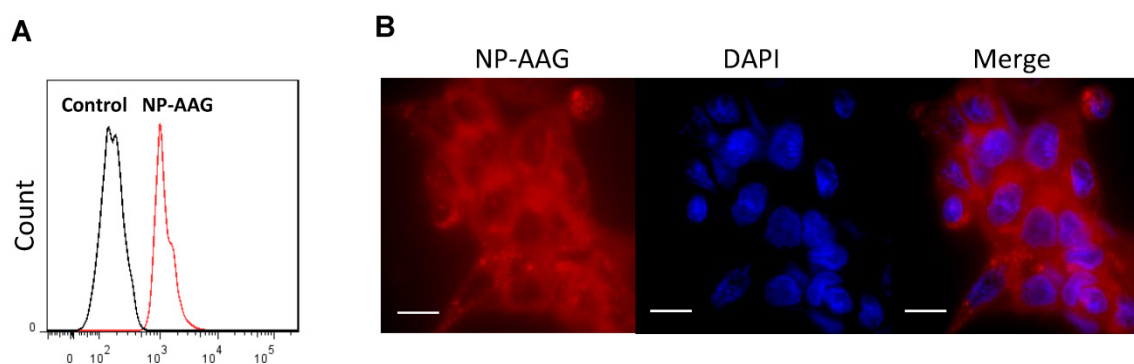


Figure 2. Cell uptake of NP-AAG by PC3 prostate cancer cells. (A) Flow cytometry evaluation of cellular uptake of NP-AAG after 20 minutes of incubation with PC3 cells. **(B)** Microscopic fluorescence imaging of subcellular distribution of NP-AAG in PC3 cells. Bar: 20 μ m; DAPI: nucleus staining.

Cellular uptake and distribution of NP-AAG in prostate cancer cells

We examined whether NP-AAG could be efficiently internalized by prostate cancer cells. PC3 cells were treated with or without NP-AAG for 20 minutes. As shown in the Fig. 2A, a significant shift in fluorescence was observed within 20 minutes by flow cytometry, indicating the uptake of NP-AAG into cells. To further investigate the biodistribution of NP-AAG at subcellular level, PC3 cells were treated with NP-AAG and cell imaging was acquired at 2 hours. NP-AAG was found mainly in the cytoplasm in a diffuse pattern with multiple scattered small aggregates (Fig. 2B). Of note, the fluorescent image was taken without removing free NP-AAG present in the culture medium. The fluorescence of intact NP-AAG in the culture medium remained quenched giving minimal background, while only those taken up by cells dissociated, leading to high fluorescent signals. These results confirmed that NP-AAG could be efficiently internalized by prostate cancer cells.

NP-AAG mediated synergistic anti-tumor effect *in vitro*

To further test the combination effect of 17AAG and nanoporphyrin-mediated PDT, we tested 2 prostate cancer cell lines (LNCAP, androgen dependent; PC3, androgen independent) and normal prostate cells (RWPE1) with an increasing concentration of 17AAG, nanoporphyrin, or NP-AAG with or without light treatments. Both PC3 and RWPE1 cells were resistant to 17AAG, while androgen dependent LNCAP cells were relatively more sensitive. This was expected as androgen receptor is a known HSP90 client protein [13] and is essential for LNCAP cell survival. Compared to normal prostate cell RWPE1, both PC3 and LNCAP cells were more sensitive to nanoporphyrin mediated PDT/PTT, while there were no cytotoxicity effects observed in all cells treated with NP without light.

Furthermore, a strong synergistic effect was observed with NP-AAG in both androgen dependent LNCAP cells and androgen independent PC3 cells (Fig. 3A, left, middle). Immortalized normal prostate cells RWPE1, however, are relatively resistant to this therapy (Fig. 3A, right). Combination indexes are < 0.3 for LNCAP and < 0.7 for PC3 cells, indicating strong synergistic effects between NP and 17-AAG (Fig. 3B). These results supported the selective anti-tumor effects of NP-AAG and synergistic effects between 17AAG and nanoporphyrin mediated PDT/PTT. Along with the imaging data in Fig. 2B, these results indicated the efficient delivery and release of 17AAG by our nanoparticles into prostate cancer cells, and its therapeutic potential against these cells.

Molecular mechanisms of NP-AAG mediated combination therapy

We intended to elucidate the mechanisms of combination therapy by NP-AAG at the molecular level. Firstly, apoptosis of PC3 prostate cancer cells was measured after treating with PBS, nanoporphyrin or NP-AAG followed by light illumination. NP-AAG mediated combination therapy caused significantly more late apoptosis (Annexin V+/PI+) than control group and nanoporphyrin mediated photo-therapy alone (Fig. 4A). This result suggested that NP-AAG mediated combination therapy induced more apoptosis mediated cell death resulting in lower cell viability. The main mechanism of nanoporphyrin mediated cytotoxicity upon light illumination is via ROS production causing oxidation and cellular damage [16]. We further investigated the ROS production of NP-AAG in PC3 cells by using DCF-DA, an indicator for intracellular ROS production, followed by light illumination. Consistent with previous findings on nanoporphyrin [16], NP-AAG could produce significant level of intracellular ROS, leading to oxidation stress and cell apoptosis/death (Fig. 4B).

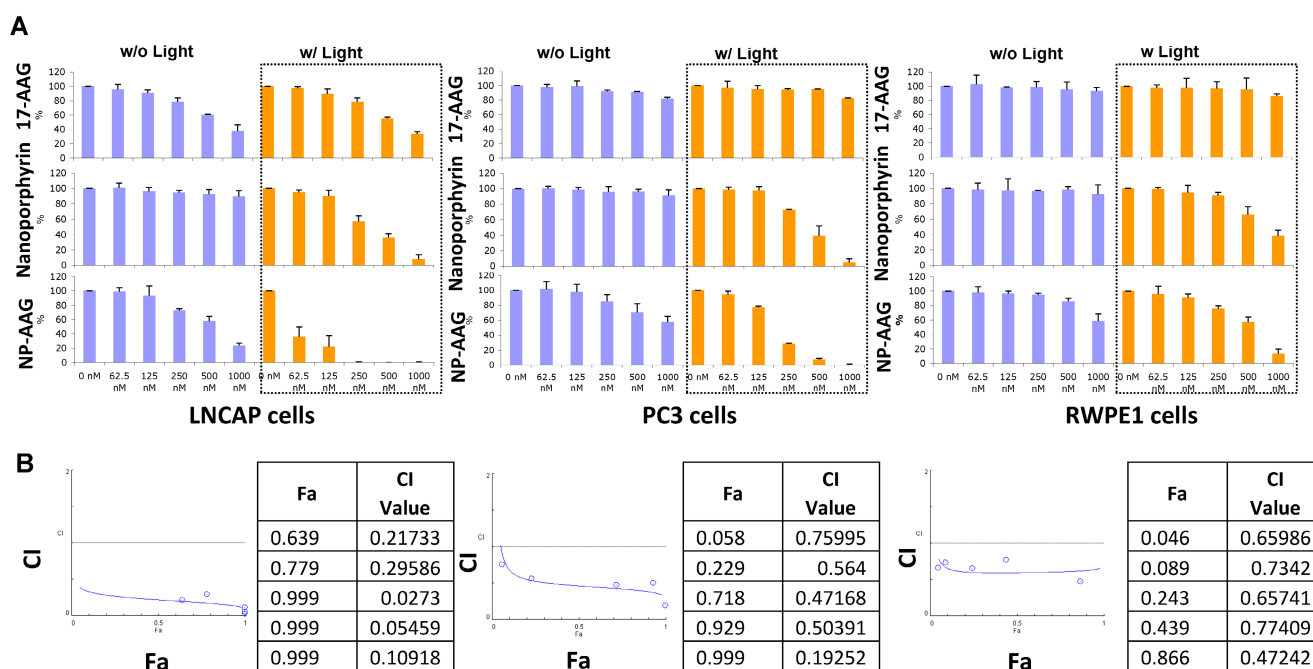


Figure 3. Viability and combination index of LNCAP, PC3 and RWPE1 cells treated with NP-AAG, nanoporphyrin alone and free drug 17AAG at various concentrations. (A) Viability of prostate cancer cells after NP-AAG treatment. Cells were seeded at 5000 cells/50µl/well and treated with the indicated drugs for 24 hrs. The drugs were removed and replaced with fresh medium, and then the cells were exposed to NIR light at 0.07 W cm⁻² for 2 min. Growth inhibition was measured using MTT assay after 72 hrs. Blue columns: no light; orange columns: with light; n=3. (B) The fraction of affect (Fa)-Combination index (CI) plots of each cell line treated with NP-AAG mediated photodynamic therapy. CI<1 is considered as synergistic, while CI <0.3 is considered as strong synergistic. CI was calculated with Compusyn software.

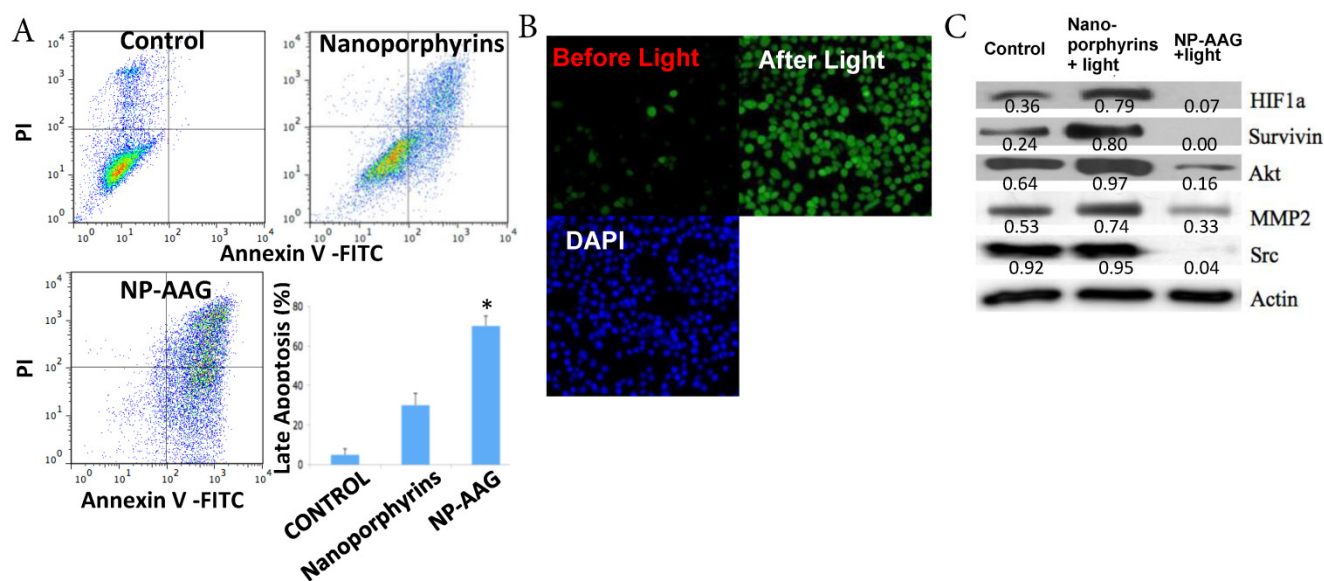


Figure 4. (A) Apoptosis of PC3 prostate cancer cells analyzed 24 hrs later using annexin V and PI staining. One representative flow cytometry result was present. Percentages of late apoptosis (Annexin V+/PI+) were graphed. Columns, mean; bars, sd; n=3. *p<0.05 **(B)** PC3 cells were treated with NP-AAG (1 mg/mL) for 24 h and loaded with DCF-DA for 30 min. Imaging was acquired before and after NIR light (0.07 W cm⁻² for 60 s) at the same field with fluorescence microscopy (20x). Green: DCF-DA fluorescence for detection of ROS production, DAPI: nucleus staining. **(C)** Molecular changes including HIF1α, survivin, AKT, MMP2 and Src levels analyzed 12 hrs later using western blot with corresponding antibodies. Protein density was measured by Image J software and the ratio of each protein and the corresponding actin was calculated and listed.

As expected, nanoporphyrin-mediated phototherapy was found to induce the expression of pro-survival and angiogenic signaling molecules, such as HIF-1α (characterized by its sustained angiogenesis), survivin (a member of inhibitor of

apoptosis protein), Akt (a key survival signaling pathway molecule) and MMP2 (associated with angiogenesis and metastasis) [1, 2, 8, 9] (Fig. 4C). There was no change in the Src level in nanoporphyrin group compared with PBS.

Nevertheless, all those onco-proteins were diminished in the NP-AAG- plus light-treated arm, as they were known as HSP90-dependent proteins (Fig. 4C). These results further demonstrated the synergistic anti-tumor effects of combination therapy via NP-AAG through inhibition of phototherapy-induced pro-survival and angiogenic proteins by *in-situ* encapsulated Hsp90 inhibitor (17AAG) in nanoporphyrins.

Imaging-guided delivery of NP-AAG

Taking advantage of the intrinsic fluorescence of NP-AAG, we could monitor the drug delivery efficiency and selectivity toward prostate tumor sites. We first evaluated the biodistribution of NP-AAG in nude mice bearing either subcutaneous or orthotopic PC3 prostate cancer xenograft by NIR fluorescence imaging. The *in vivo* imaging was acquired 72 hours

after i.v. injection of NP-AAG (Fig. 5A & B). Significant accumulation of NIR fluorescence signal from NP-AAG were noted at the tumor sites. Mice were then sacrificed and tumor, as well as other major organs were collected. *Ex vivo* imaging confirmed the selective accumulation of NP-AAG at the tumor sites, but at significantly lower levels at other major organs, such as lung, spleen, liver, fat and skin (Fig 5A, B, and C) when normalized to fluorescence signals of muscle. The preferential accumulation of NP-AAG in subcutaneous and orthotopic PC3 xenograft was likely due to the enhanced permeability and retention (EPR) effect[16]. These results confirmed the targeted drug delivery efficacy and selectivity of NP-AAG to prostate cancer tumors in both subcutaneous and orthotopic mouse prostate cancer xenograft models.

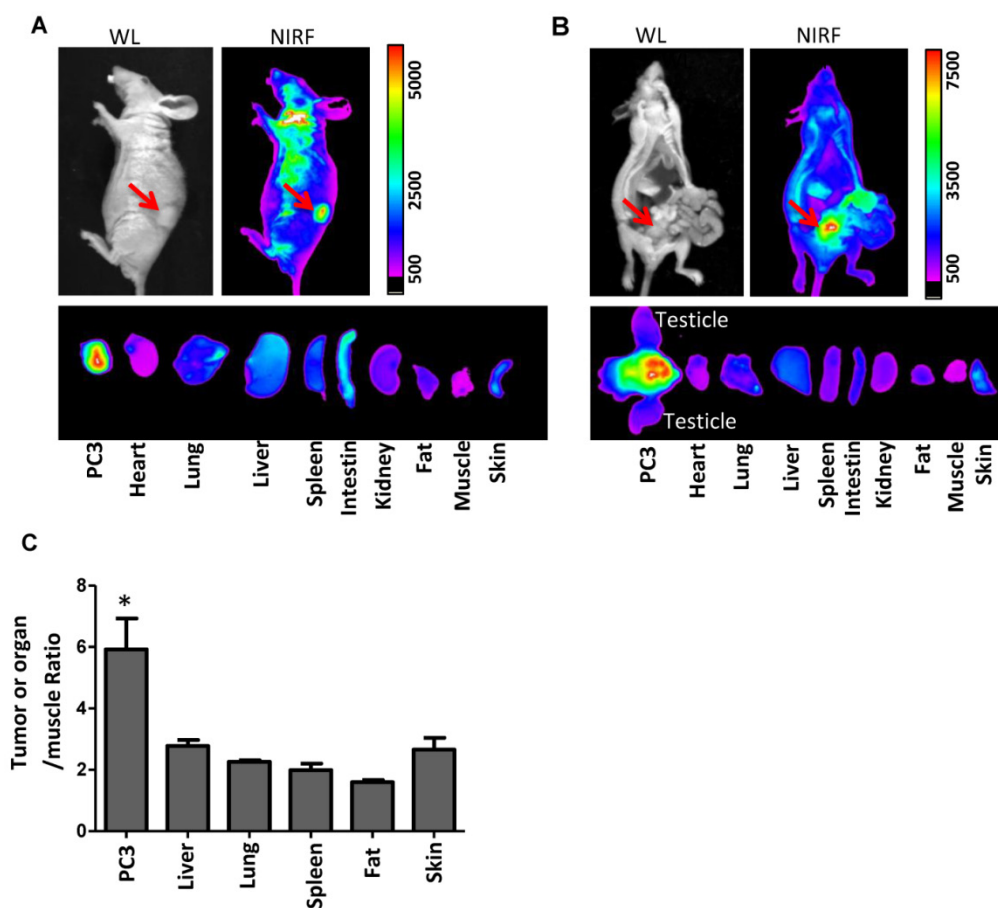


Figure 5. Imaging guided drug delivery of NP-AAG in both mouse models bearing (A) subcutaneous and (B) orthotopic PC3 xenograft. (A) *in vivo* and *ex vivo* white light (WL) and NIRF imaging of nude mice bearing subcutaneous PC3 xenograft or (B) orthotopic PC3 xenograft after 72 hours post injection of NP-AAG. Arrows: tumor site. (C) Analysis of NIRF imaging on each tumor and organs after normalization to the fluorescence of muscle. * $p < 0.05$ compared to the rest of the organs (n=3).

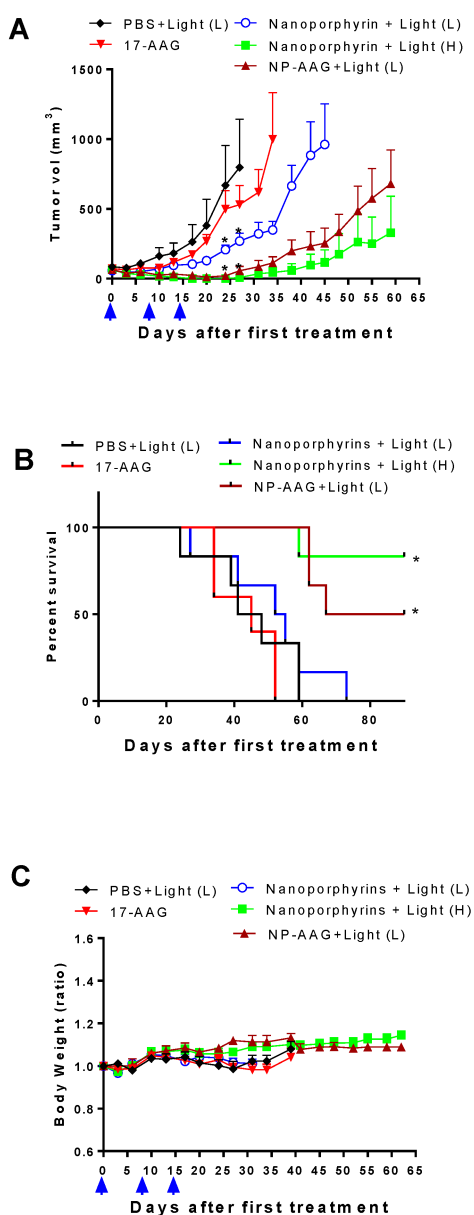


Figure 6. Tumor volume change (A), overall survival (B) and body weight change (C) of nude mice bearing PC3 prostate cancer xenograft (n=8) treated with nanoporphyrins, NP-AAG and free 17AAG on day 0, 7, and 14 (black arrows) followed by light exposure on the tumors in the mice in the mice at 24 hrs post-injection. 17AAG dose: 40 mg/kg, nanoporphyrin dose: 25 mg/kg (equivalent to 5 mg/kg of Por), Light dose: H: 1.25 W cm⁻² for 3 min, L: 0.5 W cm⁻² for 3 min.

NP-AAG mediated synergistic combination therapy *in vivo*

After confirming its drug delivery efficiency, the therapeutic efficacy of NP-AAG was further evaluated in animal models. Nude mice bearing subcutaneous PC3 xenograft were established and the treatment was initiated when tumor volume reached 100-150 mm³. Mice were treated with PBS, 17AAG free drug (dose: 40mg/kg), nanoporphyrin, or NP-AAG (17AAG dose: 40mg/kg; nanoporphyrin dose: 25 mg/kg). PBS, nanoporphyrin and NP-AAG

groups were treated with light as indicated 24 hours later. As shown in **Fig. 6A**, 17AAG alone showed minimal anti-tumor activity as its dose was relatively lower than those reported in the literature[2, 28, 29]. Nanoporphyrin alone with low dose of light (0.5W cm⁻² for 3 min) showed mild to moderate anti-tumor effect. In contrast, combination therapy via NP-AAG with low dose of light treatment was more efficacious than single treatment alone (**Fig. 6A**). In the absence of AAG, phototherapy with nanoporphyrin alone but higher dose of light (1.25 W cm⁻² for 3 min) was found to be very effective. For example, mice treated with NP-AAG plus low dose light vs nanoporphyrin plus high dose light resulted in cure of 2/6 (33.3%) and 4/6 (66.7%), respectively (**Fig. 6B**). In agreement with the efficacy study, both treatment groups with NP-AAG plus low dose of light and nanoporphyrin plus high dose of light had significantly longer medium survival, compared to PBS, 17AAG, and nanoporphyrin plus low dose of light (**Fig. 6B & Table 1**). General toxicity was monitored by the total body weight changes and there were no significant changes among groups at this dosing schedule (**Fig. 6C**). Together, our data indicated that combination therapy with NP-AAG and low dose of light was more efficacious than single treatment modality with identical dose of drug and light, resulting in prolonged survival time. Tumors collected at 24 hours post illumination from nanoporphyrin and NP-AAG groups, but not PBS and 17AAG alone groups, exhibited extensive tissue necrosis under histopathology evaluation (data not shown), indicating the photo-cytotoxic mechanism.

Table 1. Medium survival of mice treated with PBS, 17AAG, nanoporphyrin with Low/High dose of light, and NP-AAG with low dose of light, light dose: H: 1.25 W cm⁻² for 3 min, L: 0.5 W cm⁻² for 3 min, (n=6).

Groups	Medium Survival (Days)
PBS+Light (L)	44.5
17AAG	45.0
Nanoporphyrin +Light (L)	53.5
Nanoporphyrin +Light (H)	Not reached
NP-AAG+Light (L)	78.5

There was a light-dose dependent tumor inhibition upon nanoporphyrin treatment (**Fig. 6A**). We believed that this was likely due to the light-dose dependent increase of tumor temperature induced by nanoporphyrin mediated photothermal effects (**Fig. 7**). When given low dose of light for 2 minutes, tumor surface temperature was found to increase 9.7±0.6 and 10.0±1.0 °C in the nanoporphyrin and NP-AAG treated groups, respectively, whereas the PBS control

group exhibited only a $3.3\pm 0.6^\circ\text{C}$ increase. With high dose of light, tumor surface temperature increased 16.1 ± 2.0 and $16.3\pm 1.0^\circ\text{C}$ in the nanoporphyrin and NP-AAG treated groups, respectively, but only a $6.9\pm 2.0^\circ\text{C}$ increase in the PBS control group. These results demonstrated that 17AAG loading did not affect nanoporphyrin mediated heat generation upon light illumination. In the efficacy study, we also observed that 6/6 (100%) mice developed skin swelling at the irradiated tumor sites a few hours after high dose light treatment. Tumor mass decreased and turned brown-black followed by scar formation and skin healing after one week. In contrast, only 3 to 4 out of 6 mice treated with nanoporphyrin or NP-AAG with low dose of light treatment developed skin swelling. In agreement with our previous studies[16], although nanoporphyrin with high dose of light induced very effective photothermal effects, NP-AAG exhibited comparable effect with lower dose of light with less adverse effect on local skin (Fig 6A). Additionally, since our light spot generated from optical fiber did not create homogenous large light spot to cover the entire tumor area during treatment, tumor recurrence was observed from the residual tumor cells on the border of the tumor mass at later time. This challenge could be potentially overcome through careful calculation and planning with multiple optical fiber insertions into solid prostate cancers to ensure the whole tumor and margins will receive sufficient light illumination.

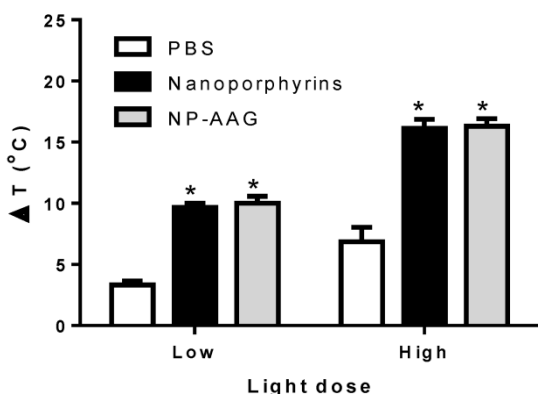


Figure 7. Light dose dependent photothermal effect in mouse xenograft models. Nude mice bearing PC3 xenograft received i.v. PBS, nanoporphyrins or NP-AAG (17AAG: 40mg/kg) for 24 hours followed by low (0.5 W cm^{-2}) and high (1.25 W cm^{-2}) dose of light for 3 minutes. Tumor surface temperature was measured by the FLIR thermal camera. * $p < 0.0001$ comparing to PBS control.

Toxicity Study of NP-AAG in nude mice bearing PC3 xenograft

In addition to body weight changes mentioned above, potential toxicities associated with all the groups were evaluated by complete blood count

(CBC), and serum chemistry (hepatic and renal function panel test) 3 days after the last dose in the efficacy study with nude mice. The CBC results showed that WBC, RBC, hemoglobin and platelet in all the treatment groups were within normal limits compared to the PBS control group (Table 2). As shown in Table 3, serum chemistry (ALT, AST, creatinine, BUN total and bilirubin) in all the groups was also within the normal range, indicating the normal hepatic and renal function after treatment with nanoporphyrin or NP-AAG. The above results indicated that our nano-formulation did not induce any significant systemic toxicity.

Table 2. CBC results of mice treated with 17AAG, nanoporphyrin, and NP-AAG followed by light treatment on the third day after the last dose, light dose: H: 1.25 W cm^{-2} for 3 min, L: 0.5 W cm^{-2} for 3 min.

	WBC (K/ μL)	RBC (M/ μL)	Hematocrit (%)	Hemoglobin (g/dL)	Platelets (K/ μL)
PBS	7.1±1.37	9.9±0.66	47.4±2.7	14.2±0.82	786±85.5
17AAG	4.9±1.73	9.1±0.32	44.2±3.2	13.6±0.50	909±78.9
Nanoporphyrin +Light(L)	6.4±1.87	8.4±0.95	40.0±3.5	12.8±1.04	931±379.1
Nanoporphyrin +Light(H)	6.6±3.79	8.7±0.43	42.5±2.4	14.0±0.68	1189±120.1
NP-AAG+Light(L)	5.9±1.96	8.5±0.44	42.0±1.5	14.0±0.47	1109±96.3

Table 3. Liver and kidney panel of mice treated with 17AAG, nanoporphyrin, and NP-17AAG followed by light treatment on the third day after the last dose, light dose: H: 1.25 W cm^{-2} for 3 min, L: 0.5 W cm^{-2} for 3 min.

	ALT (U/L)	AST (U/L)	Creatinine (mg/dL)	BUN (mg/dL)	Total Bilirubin (mg/dL)
PBS	30±6.4	85±19.4	0.14±0.02	14.5±1.68	0.13±0.03
17AAG	28±4.3	84±16.2	0.18±0.07	18.9±2.84	0.10±0.04
Nanoporphyrin +Light(L)	31±4.0	94±23.9	0.21±0.08	15.7±1.92	0.12±0.04
Nanoporphyrin +Light(H)	28±2.5	94±15.5	0.17±0.04	19.5±2.68	0.09±0.03
NP-AAG+Light(L)	31±7.1	87±4.96	0.17±0.04	17.2±1.53	0.14±0.11

Discussion

We have previously demonstrated for the first time that the “soft” organic nanoporphyrin could be activated to release heat and ROS simultaneously at tumor site for dual PTT/PDT under the irradiation of a portable, single wavelength NIR laser[16]. PTT/PDT is a minimally invasive technique for localized prostate cancer that offers the potential to destroy the cancer without making any incision or causing any potential devastating sexual, urinary or reproductive side-effects. Unlike radical prostatectomy or local radiotherapy, PTT/PDT can be repeated in case of local recurrence or a new primary tumor in the previously treated area. Such retreatment is extremely

difficult for either surgery or radiotherapy, without the risk of severe normal tissue damage[1].

Water insolubility of Hsp90 inhibitors such as 17AAG has been known as the major barrier for clinical application. The dose-limiting toxicities of geldanamycin derivative Hsp90 inhibitors are hepatotoxicity, renal failure, and gastrointestinal toxicities.[30] In this study, we successfully utilized NP nano-platform to formulate and targeted-deliver these inhibitors to improve their therapeutic efficacy and minimize their toxicities. In agreement with previous publications [1, 2, 8, 9], Hsp90 inhibitors loaded in nanoporphyrin have also been shown to decrease levels of client proteins, such as survivin, Akt, HIF1 α and MMP-2 that are raised by phototherapy, therefore, further sensitizing cancer cells to phototherapy.

Combinations of the above two novel therapeutic modalities (PTT/PDT and NP-AAG) without overlapping toxicities greatly improved the therapeutic index of treatments (**Fig. 6, Table 1-3**). Possible mechanisms of enhanced anti-tumor efficacy by combination therapy via NP-AAG are: 1) The initial release of Hsp90 inhibitors from NP-AAG sensitizes tumor cells to PTT/PDT; and 2) The sustained release of Hsp90 inhibitors from NP-AAG interferes with cyto-protective molecular responses triggered by PTT/PDT in surviving tumor or stromal cells to further enhance the efficacy. Furthermore, any interactions between PTT/PDT and NP-AAG were confined to the illuminated area. Therefore, the potentiated toxicity of the combinations is not systemic. It was also important to note that there was minimal fluorescent signal in the skin after injection of NP-AAG into mouse models (**Fig. 5**). Conventional photosensitizers tend to non-specifically accumulate at the skin and can cause severe skin burn if patients exposed to sun light after receiving those photosensitizers. Therefore, our formulation may have an advantage of minimal skin phototoxicity even given systemically.

In summary, the present research involves the development of novel nanoparticle-mediated multimodality phototherapy and molecular therapy against prostate cancer. This project addresses the critical issue in prostate cancer research for more efficacious and less toxic treatment of prostate cancer. The proposed novel multifunctional nano-platform has been demonstrated to improve prostate cancer treatment through: (i) cancer-specific and image-guided drug delivery; (ii) minimally invasive NP-mediated PTT/PDT against prostate cancer; and (iii) synergetic combination PTT/PDT and Hsp90 inhibitors that could further enhance the anti-cancer efficacy. Taken all these factors together, this novel

combination nano-medicine platform can be potentially used to effectively treat prostate cancer, prevent disease progression into invasive stages, decrease cancer recurrence and eliminate the risk from surgery or ionizing radiotherapy.

Acknowledgements

The authors thank the financial support from NIH/NCI (3R01CA115483, to K.S.L.), NIH/NIBIB (R01EB012569, to K.S.L.), DoD PRMRP Award (W81XWH-13-1-0490, to K.S.L.), NIH/NCI (R01CA199668, to Y.L.) and NIH/NICHHD (1R01HD086195, to Y.L.).

Competing Interests

Y.L., K.S.L., C.P. and T.L. are the inventors of pending patent on nanoporphyrin (US patent application US76916-856975/212300). K.S.L. is the founding scientist of LamnoTherapeutics Inc which plan to develop the nanotherapeutics described in the manuscript.

References

- Agostinis P, Berg K, Cengel KA, Foster TH, Girotti AW, Gollnick SO, et al. Photodynamic therapy of cancer: an update. *CA Cancer J Clin.* 2011; 61: 250-81.
- Ferrario A, Gomer CJ. Targeting the 90 kDa heat shock protein improves photodynamic therapy. *Cancer letters.* 2010; 289: 188-94.
- Savellano MD, Owusu-Brackett N, Son J, Ganga T, Leung NL, Savellano DH. Photodynamic tumor eradication with a novel targetable photosensitizer: strong vascular effects and dependence on treatment repetition versus potentiation. *Photochem Photobiol.* 2013; 89: 687-97.
- Lim CK, Heo J, Shin S, Jeong K, Seo YH, Jang WD, et al. Nanophotosensitizers toward advanced photodynamic therapy of Cancer. *Cancer Lett.* 2012.
- Bugaj AM. Targeted photodynamic therapy--a promising strategy of tumor treatment. *Photochem Photobiol Sci.* 2011; 10: 1097-109.
- Zhao B, He YY. Recent advances in the prevention and treatment of skin cancer using photodynamic therapy. *Expert Rev Anticancer Ther.* 2010; 10: 1797-809.
- Derycke AS, de Witte PA. Liposomes for photodynamic therapy. *Adv Drug Deliv Rev.* 2004; 56: 17-30.
- Chen B, Pogue BW, Zhou X, O'Hara JA, Solban N, Demidenko E, et al. Effect of tumor host microenvironment on photodynamic therapy in a rat prostate tumor model. *Clin Cancer Res.* 2005; 11: 720-7.
- Ferrario A, Rucker N, Wong S, Luna M, Gomer CJ. Survivin, a member of the inhibitor of apoptosis family, is induced by photodynamic therapy and is a target for improving treatment response. *Cancer Res.* 2007; 67: 4989-95.
- Kamal A, Thao L, Sensintaffar J, Zhang L, Boehm MF, Fritz LC, et al. A high-affinity conformation of Hsp90 confers tumour selectivity on Hsp90 inhibitors. *Nature.* 2003; 425: 407-10.
- Guo W, Reigan P, Siegel D, Zirrolli J, Gustafson D, Ross D. Formation of 17-allylamino-demethoxygeldanamycin (17-AAG) hydroquinone by NAD(P)H:quinone oxidoreductase 1: role of 17-AAG hydroquinone in heat shock protein 90 inhibition. *Cancer Res.* 2005; 65: 10006-15.
- Xu W, Neckers L. Targeting the molecular chaperone heat shock protein 90 provides a multifaceted effect on diverse cell signaling pathways of cancer cells. *Clin Cancer Res.* 2007; 13: 1625-9.
- Solit DB, Scher HI, Rosen N. Hsp90 as a therapeutic target in prostate cancer. *Seminars in oncology.* 2003; 30: 709-16.
- Huynh E, Zheng G. Engineering multifunctional nanoparticles: all-in-one versus one-for-all. *Wiley interdisciplinary reviews Nanomedicine and nanobiotechnology.* 2013; 5: 250-65.
- Lovell JF, Jin CS, Huynh E, Jin H, Kim C, Rubinstein JL, et al. Porphyosome nanovesicles generated by porphyrin bilayers for use as multimodal biophotonic contrast agents. *Nat Mater.* 2011; 10: 324-32.
- Li Y, Lin TY, Luo Y, Liu Q, Xiao W, Guo W, et al. A smart and versatile theranostic nanomedicine platform based on nanoporphyrin. *Nat Commun.* 2014; 5: 4712.
- Xiao K, Luo J, Fowler WL, Li Y, Lee JS, Xing L, et al. A self-assembling nanoparticle for paclitaxel delivery in ovarian cancer. *Biomaterials.* 2009; 30: 6006-16.

18. Li Y, Xiao K, Luo J, Lee J, Pan S, Lam KS. A novel size-tunable nanocarrier system for targeted anticancer drug delivery. *Journal of Controlled Release*. 2010; 144: 314-23.
19. Li Y, Xiao K, Luo J, Xiao W, Lee JS, Gonik AM, et al. Well-defined, reversible disulfide cross-linked micelles for on-demand paclitaxel delivery. *Biomaterials*. 2011; 32: 6633-45.
20. Li Y, Xiao W, Xiao K, Berti L, Luo J, Tseng HP, et al. Well-defined, reversible boronate crosslinked nanocarriers for targeted drug delivery in response to acidic pH values and cis-diols. *Angew Chem Int Ed Engl*. 2012; 51: 2864-9.
21. Rong P, Yang K, Srivastan A, Kiesewetter DO, Yue X, Wang F, et al. Photosensitizer loaded nano-graphene for multimodality imaging guided tumor photodynamic therapy. *Theranostics*. 2014; 4: 229-39.
22. Ng KK, Lovell JF, Veedadi A, Hajian T, Zheng G. Self-assembled porphyrin nanodiscs with structure-dependent activation for phototherapy and photodiagnostic applications. *ACS nano*. 2013; 7: 3484-90.
23. Chou TC. Theoretical basis, experimental design, and computerized simulation of synergism and antagonism in drug combination studies. *Pharmacological reviews*. 2006; 58: 621-81.
24. Chou TC. Drug combination studies and their synergy quantification using the Chou-Talalay method. *Cancer research*. 2010; 70: 440-6.
25. Grasso AW, Wen D, Miller CM, Rhim JS, Pretlow TG, Kung HJ. ErbB kinases and NDF signaling in human prostate cancer cells. *Oncogene*. 1997; 15: 2705-16.
26. Nguyen HG, Yang JC, Kung HJ, Shi XB, Tilki D, Lara PN, Jr., et al. Targeting autophagy overcomes Enzalutamide resistance in castration-resistant prostate cancer cells and improves therapeutic response in a xenograft model. *Oncogene*. 2014; 33: 4521-30.
27. Xiao K, Li Y, Luo J, Lee JS, Xiao W, Gonik AM, et al. The effect of surface charge on in vivo biodistribution of PEG-oligocholeic acid based micellar nanoparticles. *Biomaterials*. 2011; 32: 3435-46.
28. Vaseva AV, Yallowitz AR, Marchenko ND, Xu S, Moll UM. Blockade of Hsp90 by 17AAG antagonizes MDMX and synergizes with Nutlin to induce p53-mediated apoptosis in solid tumors. *Cell death & disease*. 2011; 2: e156.
29. de Candia P, Solit DB, Giri D, Brogi E, Siegel PM, Olshen AB, et al. Angiogenesis impairment in Id-deficient mice cooperates with an Hsp90 inhibitor to completely suppress HER2/neu-dependent breast tumors. *Proceedings of the National Academy of Sciences of the United States of America*. 2003; 100: 12337-42.
30. Workman P. Auditing the pharmacological accounts for Hsp90 molecular chaperone inhibitors: unfolding the relationship between pharmacokinetics and pharmacodynamics. *Mol Cancer Ther*. 2003; 2: 131-8.